EARTH SURFACE PROCESSES AND LANDFORMS
Earth Surf. Process. Landforms **43**, 1757–1767 (2018)

Published online 7 March 2018 in Wiley Online Library
(wileyonlinelibrary.com) DOI: 10.1002/esp.4350

Spatial modeling of pyroclastic cover deposit thickness (depth to bedrock) in peri-volcanic areas of Campania (southern Italy)

Matteo Del Soldato,[1]* Veronica Pazzi,[1] Samuele Segoni,[1] Pantaleone De Vita,[2] Veronica Tofani[1] and Sandro Moretti[1]
[1] Department of Earth Sciences, University of Firenze, Firenze, Italy
[2] Department of Earth Sciences, Environment and Resources, Federico II University of Napoli, Complesso Universitario di Monte Sant'Angelo, Napoli, Italy

Received 9 November 2017; Revised 10 January 2018; Accepted 17 January 2018

*Correspondence to: Matteo Del Soldato, Department of Earth Sciences, University of Firenze, Via La Pira, 4 - 50121 Firenze, Italy. E-mail: matteo.delsoldato@unifi.it

ESPL
Earth Surface Processes and Landforms

ABSTRACT: In this study, the main focus is the application and improvement of four empirical models, which account for the pyroclastic cover deposit thickness (PCDT) spatial distribution with respect to the bedrock surrounding the Somma-Vesuvius volcano (Campania, southern Italy). Three models, which are already known in the literature, link the depth to bedrock to the morphological features of a slope. An original model called SEPT (slope exponential pyroclastic thickness) is presented in this manuscript and combines the initial total thickness of ash-fall pyroclastic cover with the slope gradient. All models were applied and validated using field measurements derived from this and preceding studies in the study area.

The main finding is that the spatial distribution of the depth to bedrock in mountainous peri-volcanic areas mainly depends on the initial thickness of air-fallen material at a given position and slope angle. These findings allowed for the recognition of an ash-fall pyroclastic depositional environment that is characterized by different processes from those existing in other geomorphological frameworks and in which the soil thickness along the slopes is controlled by the weathering of bedrock and the formation of soil *in situ*. Finally, in this research, a reliable approach is proposed that is also applicable to other peri-volcanic areas of the world to assess the spatial distribution of the depth to bedrock, which is a fundamentally important parameter in distributed geomorphologic and hydrologic modeling. © 2018 The Authors. Earth Surface Processes and Landforms published by John Wiley & Sons Ltd.

KEYWORDS: tephra deposits; peri-volcanic areas; H/V technique; empirical models; spatial modeling

Introduction

Peri-volcanic areas are mantled with unconsolidated ash-fall deposits, which were often deposited during different stages of volcanic eruption and typically combined to form complex volcaniclastic series. Sometimes ash beds are sufficiently thick to seal off the antecedent landscape and soil (retardant upbuilding pedogenesis), and in situations typical of more distal or upwind sites, the ash deposits are thinner and ash-fall deposition and pedogenesis act together (developmental upbuilding pedogenesis) (Lowe and Tonkin, 2010). Independent of spatial organization, soils, paleosols and ash-fall deposits usually have geotechnical and hydraulic properties that are very different from the bedrock and are considered a single body, according to the engineering definition of soil (McDaniel *et al.*, 2012). The spatial distribution of pyroclastic cover deposit thickness (PCDT) with respect to bedrock is a fundamental parameter that influences several geomorphological and hydrological processes such as landscape evolution (Heimsath *et al.*, 1997; Heimsath *et al.*, 2000; Braun *et al.*, 2001), soil conservation (Schumacher *et al.*, 1999; Gabet and Dunne, 2003), hillslope hydrology (De Vita *et al.*, 2013; Napolitano *et al.*, 2015) and the triggering of shallow landslides (Johnson and Sitar, 1990; Wu and Sidle, 1995; Van Asch *et al.*, 1999; Dietrich *et al.*, 2007; Segoni *et al.*, 2012).

Along slopes, the spatial variability of PCDT is difficult to assess because it is controlled by contrasting soil forming and denudational processes, which are important factors in site-specific geomorphological environments. The international literature reports the use of many models based on simple correlations between PCDT and one specific topographic attribute, such as slope gradient or elevation (e.g. Saulnier *et al.*, 1997). Other approaches use a combination of a more complex series of different morphological attributes (DeRose, 1996; Saulnier *et al.*, 1997; Salciarini *et al.*, 2006; Segoni *et al.*, 2013). Some studies were conducted to analyze and model the temporal evolution of soil thickness (Heimsath *et al.*, 1997, 1999, 2000, 2001; Mudd and Furbish, 2004; Saco *et al.*, 2006) and demonstrated an existing relationship between the soil depth and the morphometric index of the soil transport capacity (Park *et al.*, 2001). Finally, other approaches were based on complex models using process based or multivariate statistics (Boer *et al.*, 1996; Gessler *et al.*, 2000; Tsai *et al.*, 2001; Casadei *et al.*, 2003; Pelletier and Rasmussen, 2009;

Tesfa *et al.*, 2009). Among the possible approaches, those based on independent variables that are applied to a specific site (Boer *et al.*, 1996; Tsai *et al.*, 2001) or in limited areas (Moore *et al.*, 1993; Odeha *et al.*, 1994) allowed for better results when spatially modeling soil thickness.

For the most part, literature studies have focused on analyzing the geomorphological frameworks that are characterized by a residual regolith mantle that underwent null or limited transportation by hillslope processes (i.e. soil of autochthonous origin); whereas, geomorphological environments characterized by allochthonous soil coverings have not yet been examined in depth and are limited to fewer case studies (De Vita *et al.*, 2006; De Vita and Nappi, 2013).

In this study, spatial modeling of the PCDT is proposed for the mountain slopes that surround the Somma-Vesuvius volcano (Campania, southern Italy). Three previously developed models and a new method designed purposely for this study that represents an advancement in the preceding models are compared: (a) Slope Angle Pyroclastic Thickness – SAPT (De Vita *et al.*, 2006; De Vita and Nappi, 2013); (b) Geomorphological Index Soil Thickness – GIST (Catani *et al.*, 2010); (c) Geomorphological Pyroclastic Thickness – GPT (Del Soldato *et al.*, 2016); (d) Slope Exponential Pyroclastic Thickness – SEPT (this study). These four models are used to calculate the PCDT maps and were validated against a set of measurements obtained from published papers and field surveys. The validation statistics of the four models and the spatial distribution of the residuals were used to compare the four models and to discuss the impacts of their peculiarities on the accuracy of the PCDT assessment.

Test Area Description

The study area comprises the Avella, Sarno and Lattari Mountain ranges that border the Campanian Plain (southern Italy) from the northeast to the southeast and surround the Somma-Vesuvius volcano structure, which rises in the center of the plain (Figure 1). The study area extends over approximately 3100 km^2, which includes an extensive territory with heterogeneous geomorphological features and varying physiographic features from coastal to mountainous settings.

Mountain ranges surrounding the Somma-Vesuvius volcano (Figure 2a) are characterized by a carbonate bedrock formed by Meso-Cenozoic pre-orogenetic carbonate platform series and are predominantly composed of limestone and dolomitic limestone.

Not erupted together with pyroclastic deposits erupted from the Phlegraean Fields and Somma-Vesuvius volcanoes filled the Campanian Plain and mantled its mountainous surroundings. These deposits were assembled (Rolandi *et al.*, 2000) in two groups based on their features and ages. The Ancient Pyroclastic Complex (APC) is older and was formed by ash-fall and ash-flow deposits of the Campanian Ignimbrite (39 ka BP) and of other eruptive events from the Phlegraean Fields. The Recent Pyroclastic Complex (RPC) is younger and characterized by ash-fall deposits of the Somma-Vesuvius volcano, whose activity began 25 ka BP. The most important eruptions that formed the RPC were the Sarno at 17 ka BP (Rolandi *et al.*, 2000); Ottaviano at 8 ka BP (Rolandi *et al.*, 1993a); Avellino at 3.5 ka BP (Rolandi *et al.*, 1993b); and Pompeii at AD 79 (Lirer *et al.*, 1973), AD 472 (Rolandi *et al.*, 1998), AD 1631 (Rosi *et al.*, 1993) and AD 1944 (Cole and Scarpati, 2010). Most of the eruptive events had dispersal axes that were oriented eastward, while the Pompeii eruptions at AD 79 and AD 1944 were oriented southward.

Applying lithological and pedological criteria (USDA, 1998; Terribile *et al.*, 2000), a reference stratigraphic tephra soil column found in the slope areas of Mount Sarno was recognized (De Vita and Nappi, 2013; Napolitano *et al.*, 2016) (Figure 2 b). The contents of the column from top to bottom are as follows: A – mixed mineral and organic matter; B – fine and coarse pyroclastics affected by intense pedogenesis; C – scarcely weathered pumices with fine and coarse lapilli that correspond to the Avellino eruption (3.5 ka BP); 2Bb – strongly weathered buried soil; 2C – very loose pumiceous lapilli; 3Bb – basal paleosoil with markers of intensely pedogenetic

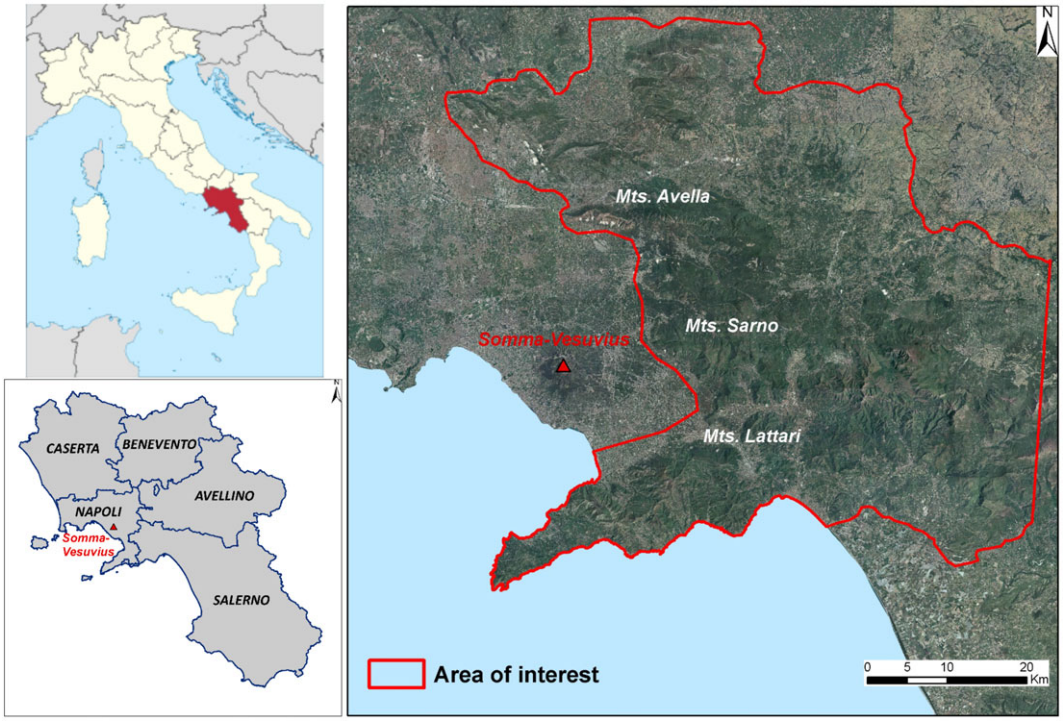

Figure 1. Localization of the mountainous area surrounding the Somma-Vesuvius volcano (red perimeter), where depth to bedrock (DTB) was investigated by field surveys and modeled. [Colour figure can be viewed at wileyonlinelibrary.com]

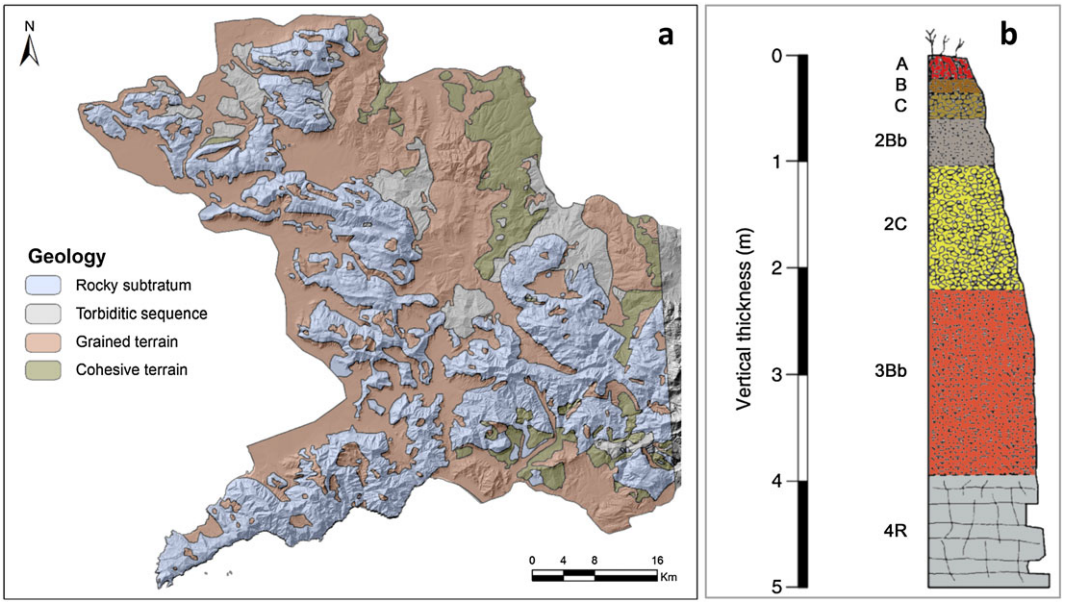

Figure 2. Geological setting of the study area (a) and complete volcaniclastic stratigraphic-soil column (modified from De Vita *et al.*, 2006) (b). A – mixed mineral and organic content; B – fine and coarse pyroclastic level affected by intense pedogenesis; C – scarcely weathered pumices with fine and coarse lapilli horizon; 2Bb – strongly weathered buried soil; 2C – very loose pumiceous lapilli; 3Bb – basal paleosoil with markers of intensely pedogenetic processes; 4R – fractured carbonate bedrock. [Colour figure can be viewed at wileyonlinelibrary.com]

processes; 4R – fractured carbonate bedrock. In the eastern sector of Mount Lattari, the volcaniclastic series is similar except for the absence of the 2Bb and 2C horizons.

The strata and soil horizon from A to 2Bb have geotechnical and hydraulic properties that are very different from those of the bedrock (4R). Ash-fall pyroclastic deposits were not distributed evenly in the study area during the eruptions. Their distribution was influenced by the distance from the vent and the orientation of the dispersal axes. In the plain areas, in which most of the stratigraphic data were collected by volcanological studies, more complete volcaniclastic column series can be found, except in sectors where fluvial erosion has truncated the stratigraphic records. However, along mountainous slopes surrounding the Campanian Plain, the thicknesses of the volcanic deposits are basically controlled by denudational and secondary depositional processes. Such erosional processes depend on the slope angle and are more enhanced for values greater than 28° (De Vita *et al.*, 2006; De Vita and Nappi, 2013). Therefore, a complete volcaniclastic series can be found in slope areas where only denudational processes and/or secondary slope depositional events (e.g. talus, colluvium or landslide deposits) are negligible. For slopes with an angle greater than 28°, a progressive reduction in ash-fall pyroclastic soil deposits and a truncation of the volcaniclastic series occur up to the approximate annulment of the pyroclastic mantle for slopes with angles greater than 50° (De Vita *et al.*, 2006; De Vita and Nappi, 2013). In peri-volcanic mountainous areas, the most important slope process is shallow landsliding, which involves ash-fall pyroclastic deposits. Landslides start from very small initial slides (debris slide) and may have a very complex downslope evolution involving debris avalanches and debris flows (Hungr *et al.*, 2001; De Vita and Piscopo, 2002; Fiorillo and Wilson, 2004; Jakob *et al.*, 2005; De Vita *et al.*, 2006; Napolitano *et al.*, 2015). The contrasting properties between bedrock and soil horizons and PCDT and slope angle represent the main factors controlling the susceptibility and timing of the onset of initial debris slides as well as the subsequent flow-like evolutionary stages.

Data and Methodology

Three models already known in scientific literature were applied (a) to evaluate the existing approaches for mapping the PCDT, (b) to understand the principal controlling factors, and (c) to identify a new, improved procedure to assess the PCDT (Figure 3). Subsequently, a new model was proposed to refine the parameters controlling the spatial variability of ash-fall pyroclastic mantle thickness.

The first step was the collection of the digital elevation model (DEM), which was a 10 cm × 10 cm cell size obtained through the TINITALY/01 DEM Project (Tarquini *et al.*, 2012); the elaboration of the DEM using spatial analysis tools in a geographic information system (GIS) environment allowed for the extraction of terrain derivative maps and field measurements collected by direct and indirect techniques (Figure 4e). The profile curvature (Figure 4a), slope (Figure 4b) and position index (Figure 4c) were evaluated and used for spatial modeling of the PCDT.

According to the allochthonous origin of the ash-fall pyroclastic deposits, the map of the initial thicknesses of the APC and RPC deposits, named z_0, was another fundamental factor under consideration in the modeling. The earlier-mentioned map was estimated by the sum (De Vita *et al.*, 2006; De Vita and Nappi, 2013) of the isopach maps (Figure 4d) created using the volcanological studies for the ash-fall pyroclastic products of the Campanian Ignimbrite (Perrotta and Scarpati, 2003) and the principal eruptions of the Somma-Vesuvius volcano (Lirer *et al.*, 1973; Rolandi *et al.*, 1993a, 1993b, 1998, 2000; Rosi *et al.*, 1993; Cole and Scarpati, 2010).

Field measurements of thickness

In the study areas, 300 field measurements of PCDT were carried out in preceding studies (De Vita *et al.*, 2006, 2007) using direct measures (trial pits and dynamic penetrometer tests) and indirect measures (resistivity and seismic refraction

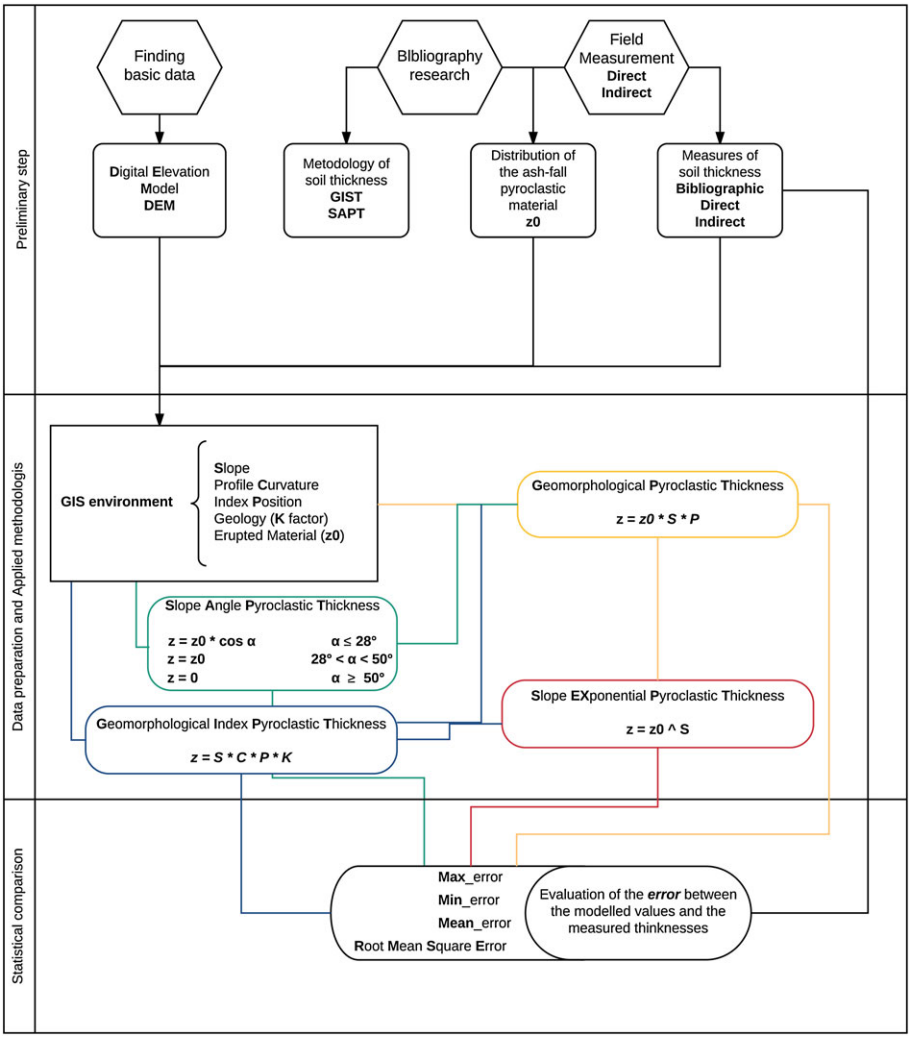

Figure 3. Flowchart of the adopted procedure to analyze the previous developed models and test the advanced one. [Colour figure can be viewed at wileyonlinelibrary.com]

soundings). These data were integrated with some new, direct measurements of the depth to bedrock (DTB), which were executed by trial pits, dynamic penetrometric tests, and horizontal-to-vertical (H/V) measures (Nakamura, 1989). In the past few years, the H/V ambient noise technique has been widely used to reconstruct geophysical and geological models and to study the interactions between soil and buildings (Pazzi *et al.*, 2016a, 2016b, 2017b). This technique is one of the most suitable geophysical methods for estimating the fundamental or resonance frequency of soft deposits and for detecting the depth to bedrock (Lane *et al.*, 2008). In practice, H/V curves show several peaks that are caused by the presence of alternating seismic horizons with different seismic velocities and likely lithologies (Pazzi *et al.*, 2017a, and references cited within), such as the condition represented by a loose ash-fall pyroclastic deposit overlying a carbonate bedrock. When the depth of the first layer or its V_S value is known, passing from the H/V-frequency domain to the depth-V_S domain to reconstruct geophysical and geological models is possible (Figure 5). In the study area, 44 measurement stations of ambient noise H/V were set to improve the PCDT dataset for direct analysis (yellow dots in Figure 4e). These measurements were acquired by means of three Tromino®, which consist of 24-bit, three-component broadband seismometers developed by the MoHo Company. To calibrate the H/V measurements and correlate the thicknesses obtained through seismic surveys with other available thicknesses, some H/V measurements were carried out at the same sites as the ash-fall pyroclastic thickness direct measurements. Each acquisition ran for 20 minutes at 256 Hz. The recorded traces were analyzed according to the SESAME Project (2004), and a local seismic stratigraphic model was reconstructed by means of the Grilla® software (Pazzi *et al.*, 2017a).

Between the existing literature and new PCDT data, a dataset of 300 measurements was formed that was used to calibrate the models and test their effectiveness. The PCDT values obtained from trial pits and dynamic penetrometer tests, which were executed along the vertical direction, were geometrically elaborated to consider the stratigraphic thickness and assessed as the projection normal to the slope surface. Furthermore, variable stratigraphic settings of the volcaniclastic series were assessed by test pits in which the different spatial conditions were recognized depending on the distance from the Somma-Vesuvius volcano and different dispersal axes of volcanic eruptions.

GIST model

The first model applied to evaluate the PCDT was the GIST model (Catani *et al.*, 2010). GIST was devised for areas with soils derived from the dominant weathering processes of bedrock (Mercogliano *et al.*, 2013; Segoni *et al.*, 2013), but it was also applied to areas covered by ash-fall pyroclastic deposits (Rossi *et al.*, 2013). The GIST approach is an empirical model that combines morphometric attributes with geomorphological and

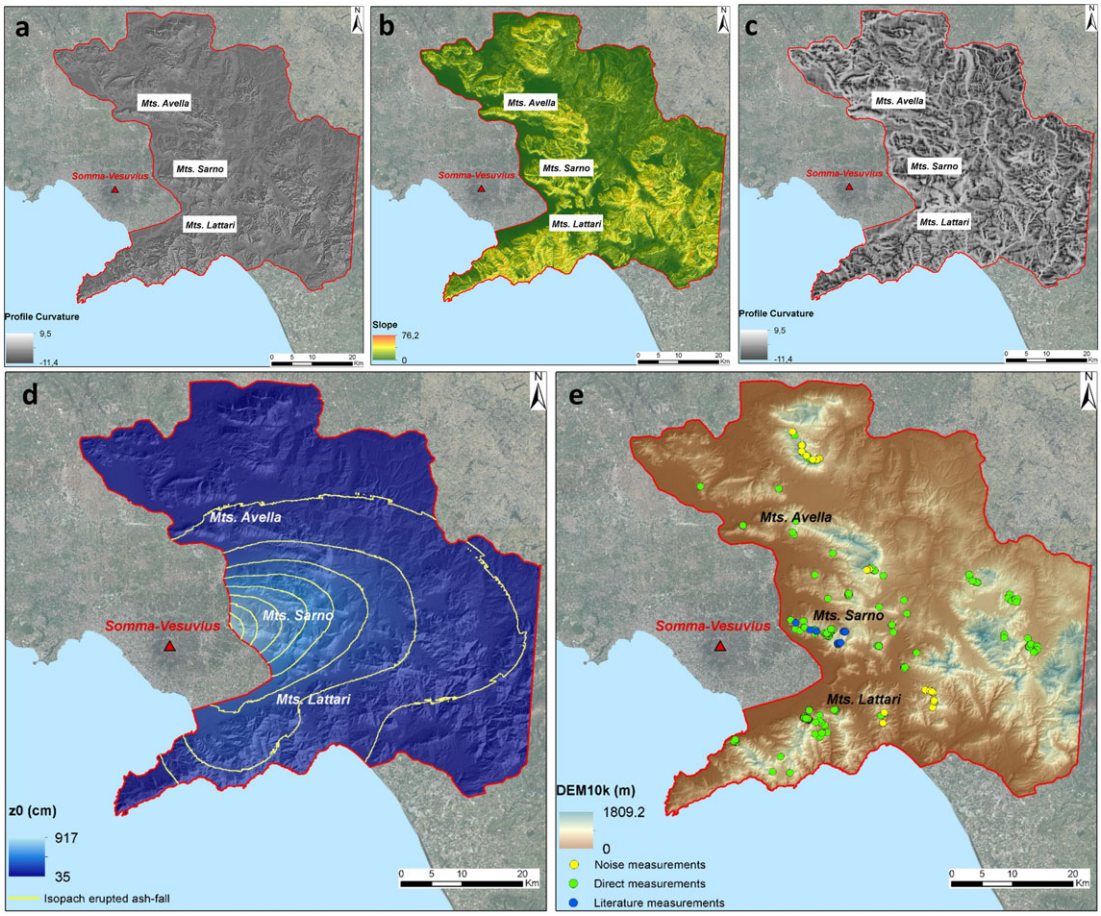

Figure 4. Profile curvature (a), slope angle (b) and position index (c) parameters involved in the spatial modeling of the depth to bedrock (DTB) in addition to the erupted material (z_0) (d), with the isopach erupted volcaniclastic material contour lines every 100 m interval and the field measurements located on the digital elevation model (e). [Colour figure can be viewed at wileyonlinelibrary.com]

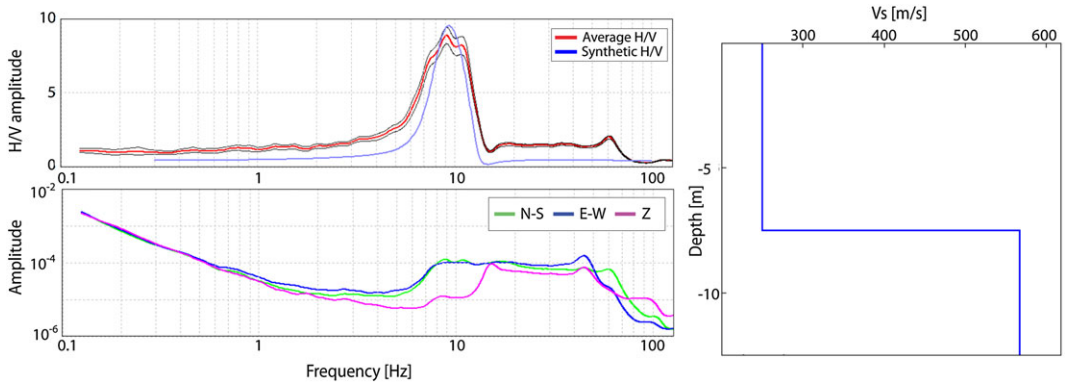

Figure 5. Sample analysis and elaboration carried out on the H/V ratio of the ambient-noise to estimate the depth to bedrock (DTB). [Colour figure can be viewed at wileyonlinelibrary.com]

geological features (Catani *et al.*, 2010). The model is based on three factors (*S*, *C* and *P*) with values ranging from 0 to 1, and these values account for the tendency to have a thicker soil:

- slope gradient (*S*), which is given by the following equation (Equation 1)

$$Slope\ Gradient_{(0-1)} = \frac{1}{1 + \tan(slope\ angle)};$$

- profile curvature (*C*), which accounts for the accumulation of material in the lower part of the slope due to erosional processes and/or mass movements;
- position index (*P*) was calculated for each pixel of the DEM as the ratio of the distance between the *i*th-point, top of the slope and length of the entire slope. The obtained values range between 0 and 1.

The assumed amounts at every pixel based on each factor depend on the local value of the corresponding morphometric attributes (curvature for factor *C*, position along the hill slope profile for factor *P* and slope gradient for factor *S*), but the relationship linking the morphometric attribute with the corresponding factor is not constant over the entire test area. The *C* values are basically assumed to be inversely dependent on

the slope curvature feature, except where the geomorphologic surveys highlight a direct proportionality (e.g. large accumulations of loose material at the footslopes). To devise factor *P*, the area is divided according to the toposequences characterizing the hillslopes, and for each subdivision, the relationship linking factor *P* and the hillslope position is independently calibrated. Factor *S* reduces the soil thickness values (proportionally to the local slope gradient) when the local gradient exceeds a threshold, which is different for every lithological class encountered in the area. The product of the three factors is then converted into a value of PCDT by means of calibration functions, which should be differentiated on a lithological basis and defined by means of *in situ* soil thickness measurements. For further details, see Catani *et al.* (2010). By considering the kinematic stability of the soil covering, the GIST approach succeeds in modeling relevant PCDT values, even in flat and concave areas (Figure 6).

The position index is fundamental, and the points along a slope having the same curvature and the same slope gradient can show important dissimilarities that are caused by their different distances from the top of the mountain. Finally, the GIST model uses the geological factor (K_i) for calibrating the earlier mentioned parameters to field measurements of thickness (PCDT), which assumes the following form (Equation 2).

$$\mathrm{DTB} = S \times C \times P \times K_i$$

In our case study, a single calibration index was considered for the entire study area because of the homogeneous lithology of the bedrock.

SAPT model

The second model applied was the SAPT (De Vita *et al.*, 2006; De Vita and Nappi, 2013), which is based on the initial total thickness (z_0) map reconstruction of ash-fall pyroclastic material erupted from the Somma-Vesuvius volcano and subordinately from the Phlegraean Fields and is obtained by summing the isopach maps of the principal eruptions. The estimated thickness (PCDT) along mountain slopes was obtained by linking the z_0 map with the slope angle (α) using the following equation (Equation 3):

$$\mathrm{DTB} = z_0 \times \cos\alpha$$

Such a theoretical model was considered a reference for comparison with field measurements of PCDT. Using this comparison, which is made for the sample areas of Mount Sarno and Mount Lattari (De Vita *et al.*, 2006, 2007; De Vita and Nappi, 2013), a good match between the real thickness observed along the slopes and the initial thickness (Equation 3) was found in the slope angle range lower than 28°. For slope angle values greater than 28°, the measured thickness showed a decreasing trend, which determined the annulment of the ash-fall pyroclastic material for slope angles that were approximately greater than 50°. The marked divergence between the trend obtained using field measurements and the theoretical model (Equation 3) was determined mainly by the effects of landsliding. The reduction in volcaniclastic material to the downslope annulment effected the stratigraphic setting because it determined the downslope pinching out of pyroclastic horizons, especially pumiceous lapilli, and hydrological conditions, which led to a localized buildup of pore pressure and triggered the initial debris slide (De Vita *et al.*, 2007; De Vita and Nappi, 2013).

The coupling of the theoretical model (Equation 3) for the slope angle range of up to 28°, the empirical model for the slope angle between 28° and 50°, and the null value for the slope angle greater than 50° was considered a reliable approach to predict the PCDT values for the peri-volcanic mountain slopes surrounding the Campanian Plain (De Vita *et al.*, 2006).

GPT model

The two previously described models were merged into the GPT model (Del Soldato *et al.*, 2016). The GPT model is characterized by an integration of the GIST model (Catani *et al.*, 2010) with the parameter used in the SAPT model (De Vita and Nappi, 2013), which represents the initial total thickness of ash-fall deposits that fell around the mountainous peri-volcanic areas. Therefore, in the GIST model, the slope gradient (*S*) and profile curvature (*C*) were maintained as representative of the morphological factors, the position index (*P*) was excluded, and the regional distribution of the initial thickness (z_0) was substituted for geological factor K_i, which is shown in Equation 4:

$$\mathrm{DTB} = C \times s \times z_0$$

The use of z_0 instead of the *K* factor is supported by the allochthonous origin of ash-fall pyroclastic material that does not depend on the lithological features of bedrock (De Vita *et al.*, 2007). Moreover, the position index (*P*) was shown to have no influence on the PCDT due to the peculiar distribution process of such deposits along slopes, which depend on the tephra fall mechanism in peri-volcanic areas (Fisher and Schmincke, 2012) and denudational processes acting along slopes.

SEPT model

To understand the fundamental parameters controlling the PCDT spatial distribution and develop a new, improved model, the GIST (Catani *et al.*, 2010), SAPT (De Vita *et al.*, 2013) and GPT (Del Soldato *et al.*, 2016) approaches were applied, and their results were mutually compared. Because of this comparison, the SEPT model is proposed in this paper, the results of which were analyzed and statistically compared with those of the other models. Because of the analytical comparison of the

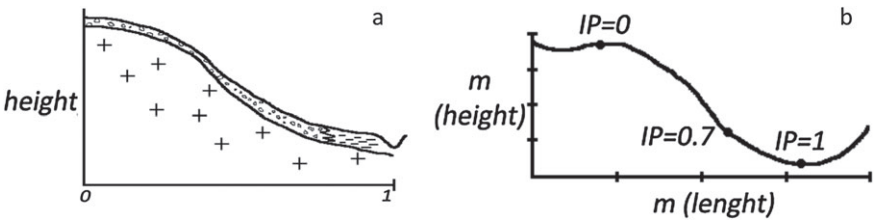

Figure 6. Relationship between the profile curvature and the bedrock depth (a). Evolution of the position index (IP) along the slope (b). IP assigns value 0 on the top of the slope and progressively increasing values going to the valley that shows 1 (Segoni, unpublished thesis, 2004).

PCDT maps obtained through the previously described methods, the actual thickness of ash-fall pyroclastic soils along slopes is controlled more by the initial total thickness (z_0) and slope gradient than by other morphological factors, such as the profile slope curvature and the position along the slope. Taking advantage of these results, the SEPT model was developed to improve the distributed modeling of the PCDT in the peri-Vesuvian area, which exclusively focused on the link between the initial total thickness of the ash-fall pyroclastic deposits (z_0) and the slope gradient. Different types of relationships between the erupted material and slope gradient were tested. Among these, an inverse exponential relation was found that best fit the field thickness data (Equation 5):

$$\mathrm{DTB} = z_0^{-\frac{1}{1+\tan(\alpha)}}$$

Results

The SAPT (Figure 7a), GIST (Figure 7b), and GPT (Figure 7c) approaches were applied to the test site, and GIS was used to obtain the PCDT distribution maps (Figure 7). Based on the analysis of the obtained results, the SEPT approach was developed as an improvement of the SAPT and GPT models (Figure 7d).

The four maps were tested by a comparison with 300 PCDT direct and indirect measurements, and residuals among field and modeled values were statistically analyzed to assess the efficiency of the results.

The modeling obtained by the GIST approach revealed the most important differences in comparison to the measured thicknesses. The SAPT model, which assumes that different empirical relationships exist in three slope ranges (up to 28°, between 28° and 50° and over 50°), was recognized as having an appreciable precision in predictions. The GPT model provided good results except for overestimation in areas far from the Somma-Vesuvius volcano and a slight underestimation in zones close to the volcano (Del Soldato *et al.*, 2016). Conversely, the SEPT model had the best match between the calculated and measured values, except that it underestimated and overestimated the values more than the GPT and SAPT approaches, respectively.

The obtained PCDT maps were statistically compared by analyzing the differences, namely, the residuals errors, among the computed and measured PCDT at 300 sites where direct and indirect field measurements were carried out. To compare computed values and field measurements, the PCDT were transformed in terms of real thickness and in a normal direction with respect to the slope surface. Descriptive statistics of residuals, which consist of the maximum overestimation and underestimation, mean and standard deviation were calculated to evaluate the efficiencies of the applied approaches for the particular area of investigation. Furthermore, the root mean square error (RMSE) was computed to assess the

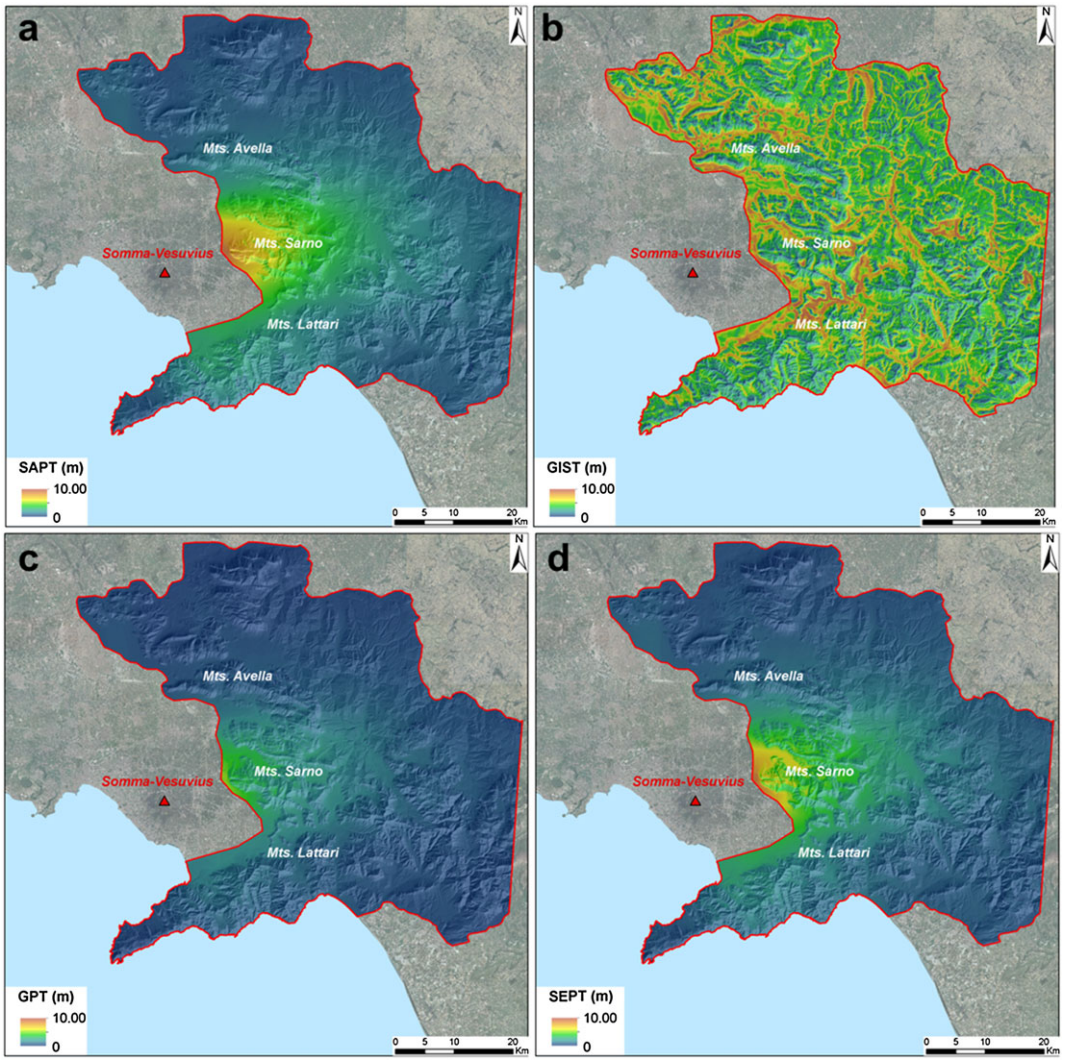

Figure 7. Distribution maps of the depth to bedrock (DTB) maps by SAPT (a), GIST (b), GPT (c) and SEPT (d) models. [Colour figure can be viewed at wileyonlinelibrary.com]

effectiveness and consistency of the tested methodologies (Table I). The lowest mean, standard deviation and RMSE values were achieved for the new SEPT model, even when the maximum and minimum residuals were higher than those of the other models.

To better clarify the different obtained results and the reliability of the new SEPT model, the residual values of each measurement point were plotted for the four models and are shown in Figure 8. It is evident that the GIST model (Figure 8 b) underestimates the PCDT in sectors far from the eruption source and overestimates it in sectors where the accumulation is more abundant, which is presumably close to the source or in the valley floor. A similar problem of overestimation is recognizable in the GPT approach, which shows a relevant extension of this effect (Figure 8c). Moreover, the SAPT model, which is based on an empirical correlation with slope angle, shows generally good results but with very localized overestimations (Figure 8a). The new SEPT model shows a better estimation for the PCDT (Figure 8d), and the residual distribution does not show systematic patterns.

Table I. Statistics of the residuals between the measured (meas) and modeled PCDT

	Meas – SAPT (m)	Meas – GIST (m)	Meas – GPT (m)	Meas – SEPT (m)
MAX_Underestimation	−5.87	−7.37	−1.68	−3.22
MAX_Overestimation	5.41	7.30	7.20	6.20
MEAN_Err	1.26	2.14	*1.08*	**0.97**
DEV.ST_Err	*1.03*	1.63	1.20	**0.88**
MSE	2.66	7.22	*2.62*	**1.72**
RMSE	1.63	2.69	*1.62*	**1.31**

The best values obtained with the use of the three known empirical approaches (SAPT, GIST and GPT) are shown in italic typeface, and the values obtained by the newly proposed SEPT empirical method are shown in bold typeface.

Discussion

The analysis of results obtained using the four tested models clearly shows that the most reliable PCDT map was calculated using the SEPT model, and the least accurate map was calculated using the GIST model; the other two models had intermediate accuracies. The GIST model showed the worst performance because it was originally designed for use in geomorphological frameworks with dominant autochthonous soil coverings produced by bedrock weathering processes and consist of *in situ* and transported regolith (Taylor and Eggleton, 2001). The latter result is related to areal denudational and depositional processes acting along slopes such as sheet-wash and rill erosion as well as the areal mass transport due to soil creep. However, in a peri-volcanic

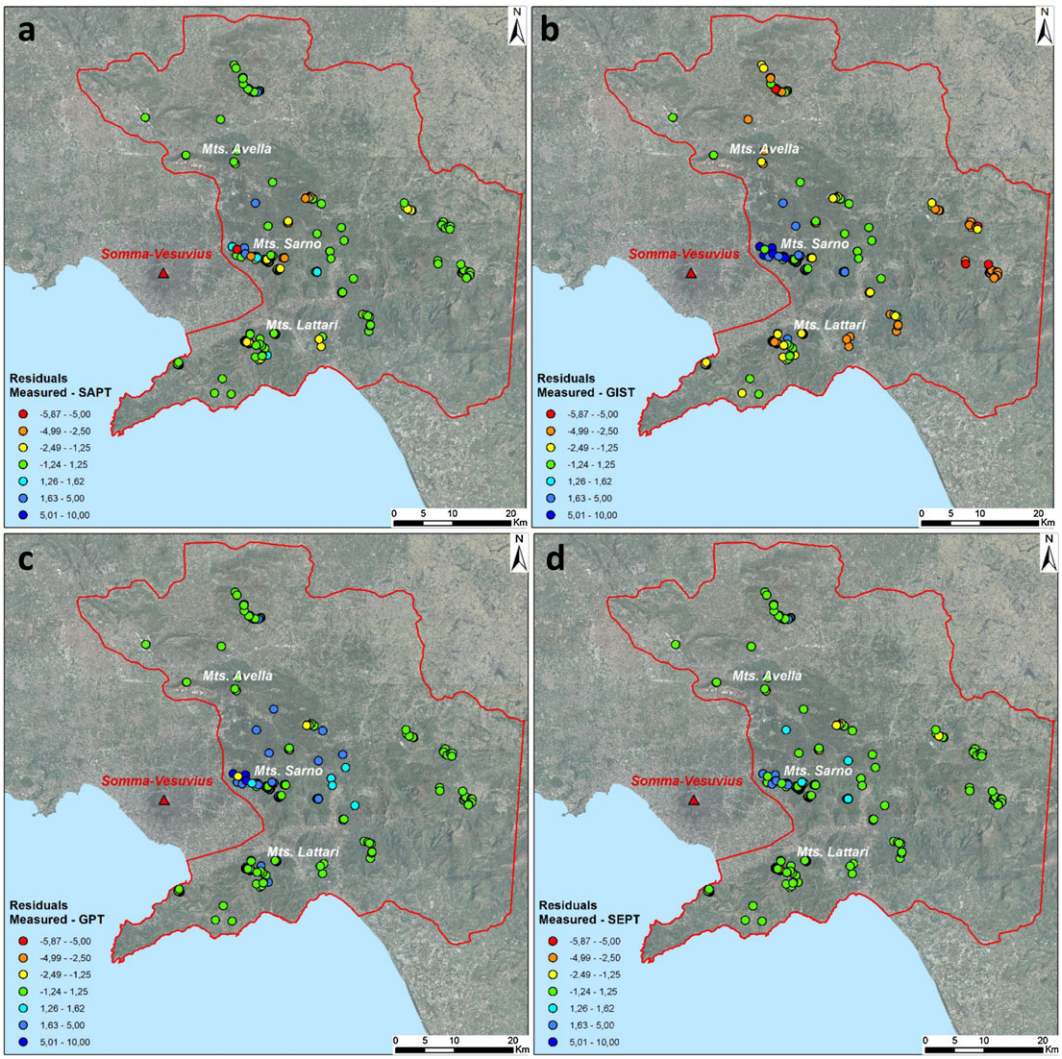

Figure 8. Residual value of the depth to bedrock (DTB) maps between the measures and the SAPT (a), GIST (b), GPT (c) and SEPT (d) models. [Colour figure can be viewed at wileyonlinelibrary.com]

geomorphological framework, such as that of the studied case, the soil covering is of allochthonous origin, that is, it is derived from pyroclastic ash-fall deposits mantling the original topography (Fisher, 1985; Sparks *et al.*, 1992). For this reason, the models with the best performances were constrained by the total thickness of the volcaniclastic material that had fallen in a given location (z_0) and were estimated by the sum of isopach maps for the principal eruptions (De Vita *et al.*, 2006; De Vita and Nappi, 2013 (Fusco *et al.*, 2017). Nevertheless, even if z_0 is a common feature for SAPT, GPT and SEPT, the conceptual difference among these models is the parameterization of the spatial distribution of PCDT along the slopes. For example, the GPT model was based on the integration of the SAPT and GIST approaches. Therefore, this approach also considers the position index and curvature of a slope (as for the GIST model). Thus, improved results were obtained, but a thorough analysis demonstrates that the main controlling parameters of the PCDT spatial distribution were limited to z_0 and slope gradient. Moreover, based on the statistical analysis of the resulting PCDT maps obtained by the SAPT and GPT models, some systematic errors were highlighted, and consequently, the new SEPT model was developed. The SEPT model advances previous models by considering only z_0 and slope gradient (α), which is similar to the SAPT model but emphasizes the role of the latter by introducing an exponential function. Validation and statistical investigations of the resulting map proved that the SEPT model estimates the PCDT distribution with a higher precision than those of the three other tested methods. For example, the standard deviation, RMSE errors, and distribution of residuals derived using a comparison with field measurements demonstrate that the SEPT model provides better results than the other tested models.

Because models that estimate the PCDT are generally excessively simplified when only based on a few parameters, for the study area, the application of different approaches led to the recognition of the fundamental role played by the slope gradient instead of other morphological variables such as slope position index and curvature. This can be related to the peculiar air-fall depositional mechanism of volcaniclastic material and the characteristics of limestone bedrock, in which weathering occurs in the form of chemical dissolution instead of decomposition and disintegration processes (Selby, 1982). The coupling of these conditions leads to the existence of a negligible weathering profile at the bedrock cap and of an allochthonous volcaniclastic soil mantle covering the bedrock. Therefore, in such a peri-volcanic landscape, the PCDT pyroclastic mantle is spatially dependent on the total depth of the erupted material that has fallen at a particular site (z_0) and by denudational processes, which mainly depend on shallow landsliding and are controlled by the slope gradient. Thus, the approach developed and proposed in this work is applicable for evaluating the PCDT of other peri-volcanic areas in the world.

Except for the preceding attempts (De Vita *et al.*, 2006; De Vita and Nappi, 2013; Del Soldato *et al.*, 2016) already discussed, no other studies were carried out to model the spatial distribution of ash-fall pyroclastic soils along steep mountainous slopes; for the most part, these studies focused on volcanological aspects and analyzed only plain and footslope sectors of peri-volcanic areas, in which the stratigraphic data were more easily accessible (e.g. Sparks *et al.*, 1992; Vogel and Märker, 2013).

Finally, the results obtained by testing the four models can help advance the understanding of the formation and spatial distribution of soil mantles covering slopes in peri-volcanic mountainous areas, such as those studied in this work. These areas are characterized by very steep slopes, and the principal denudation mechanism is related to mass movements due to shallow landsliding. In addition, creep-like processes play a minor role. Therefore, in such a geomorphological framework, the slope gradient exerts a principal role in modeling the spatial distribution of soil thickness (Aleotti and Chowdhury, 1999; Segoni *et al.*, 2009; Catani *et al.*, 2010). Conversely, a wide array of studies link the soil thickness and curvature in hillslope systems, which are dominated by creep-like processes (e.g. Heimsath *et al.*, 1999, 2001; Catani *et al.*, 2010). This finding is consistent with studies demonstrating that creep-like processes are predominant at low slope gradients and that the creep progressively loses relevance in favor of shallow landsliding as the slope gradient increases, which in turn becomes the only predominant process beyond a threshold value of the slope (e.g. Roering *et al.*, 1999).

Conclusions

In this research, a new empirical model (SEPT), which is used to assess the spatial distribution of PCDT in peri-volcanic areas, was applied to the area surrounding the Somma-Vesuvius volcano (Campania region, southern Italy). This model was compared to the results of three previously developed models (SAPT, GIST and GPT). The four PCDT maps were validated against a dataset of direct and indirect field measurements. Statistical analyses of the average and standard deviation of the error, the difference between the measured values and the respective values obtained by the models, and RMSE demonstrated that the SEPT model was the most efficient. The analysis of the spatial distribution of residuals strengthens this conclusion, as the SETP, PCDT map does not seem to be affected by systematic overestimations or underestimations.

The most important result of this research is related to the very relevant applications of PCDT mapping such as the assessment of debris flow susceptibility and hazards using heuristic and deterministic approaches, respectively, or the evaluation of the volume of potentially unstable volcaniclastic material for the estimation of runout scenarios. Therefore, the results can be considered as an important improvement in understanding shallow landslide susceptibility and can be used in physically based approaches to investigate the triggers of, shallow landslides. The analysis of the spatial distribution of the PCDT presented in this work, besides the practical applications, can also be used to advance the understanding of geomorphological processes that exist on peri-volcanic hillslopes around the world.

Acknowledgements—This research was supported by the PRIN Project (2010-2011) 'Time-Space prediction of high impact landslides under changing precipitation regimes', funded by the Ministry for Education, University and Research (MIUR-Italy).

References

Aleotti P, Chowdhury R. 1999. Landslide hazard assessment: summary review and new perspectives. *Bulletin of Engineering Geology and the Environment* **58**: 21–44.

Boer M, Del Barrio G, Puigdefábres J. 1996. Mapping soil depth classes in dry Mediterranean areas using terrain attributes derived from a digital elevation model. *Geoderma* **72**: 99–118.

Braun J, Heimsath AM, Chappell J. 2001. Sediment transport mechanisms on soil-mantled hillslopes. *Geology* **29**: 683–686.

Casadei M, Dietrich W, Miller N. 2003. Testing a model for predicting the timing and location of shallow landslide initiation in soil-mantled landscapes. *Earth Surface Processes and Landforms* **28**: 925–950.

Catani F, Segoni S, Falorni G. 2010. An empirical geomorphology-based approach to the spatial prediction of soil

thickness at catchment scale. *Water Resources Research* **46**: W05508.

Cole PD, Scarpati C. 2010. The 1944 eruption of Vesuvius, Italy: combining contemporary accounts and field studies for a new volcanological reconstruction. *Geological Magazine* **147**: 391–415.

DeRose RC. 1996. Relationships between slope morphology, regolith depth, and the incidence of shallow landslides in eastern Taranaki hill country. Zeitschrift fur Geomorphologie Supplementband: 49–60.

De Vita P, Piscopo V. 2002. Influences of hydrological and hydrogeological conditions on debris flows in peri-vesuvian hillslopes. *Natural Hazards and Earth System Science* **2**(1/2): 27–35.

De Vita P, Agrello D, Ambrosino F. 2006. Landslide susceptibility assessment in ash-fall pyroclastic deposits surrounding Mount Somma-Vesuvius: application of geophysical surveys for soil thickness mapping. *Journal of Applied Geophysics* **59**: 126–139.

De Vita P, Di Clemente E, Rolandi M, Celico P. 2007. Engineering geological models of the initial landslides occurred on April 30 2006, at Mount di Vezzi (Ischia Island, Italy). *Italian Journal of Engineering Geology and Environment* **2**: 119–141.

De Vita P, Napolitano E, Godt J, Baum R. 2013. Deterministic estimation of hydrological thresholds for shallow landslide initiation and slope stability models: case study from the Somma-Vesuvius area of southern Italy. *Landslides* **10**: 713–728.

De Vita P, Nappi M. 2013. Regional distribution of ash-fall pyroclastic soils for landslide susceptibility assessment. In *Landslide Science and Practice*. Springer: Berlin; 103–109.

Del Soldato M, Segoni S, De Vita P, Pazzi V, Tofani V, Moretti S. 2016. Thickness model of pyroclastic soils along mountain slopes of Campania (southern Italy). In *Landslides and Engineered Slopes. Experience, Theory and Practice: Proceedings of the 12th International Symposium on Landslides*, Napoli, Italy, 12–19 June 2016. CRC Press: Boca Raton, FL; 797–804.

Dietrich W, McKean J, Bellugi D, Perron T. 2007. The prediction of shallow landslide location and size using a multidimensional landslide analysis in a digital terrain model. In Proceedings of the fourth international conference on debrisflow hazards mitigation: Mechanics, prediction, and assessment (DFHM-4). Chengdu, China (pp. 10-13).

Fiorillo F, Wilson RC. 2004. Rainfall induced debris flows in pyroclastic deposits, Campania (southern Italy). *Engineering Geology* **75**: 263–289.

Fisher RV. 1985. *Pyroclastic rocks*. Springer, 472 pp.

Fisher RV, Schmincke H-U. 2012. *Pyroclastic Rocks*. Springer Science & Business Media: Berlin.

Fusco F, Allocca V, De Vita P. 2017. Hydro-geomorphological modelling of ash-fall pyroclastic soils for debris flow initiation and groundwater recharge in Campania (southern Italy). *Catena* **158**: 235–249.

Gabet EJ, Dunne T. 2003. A stochastic sediment delivery model for a steep Mediterranean landscape. *Water Resources Research* **39**: 1237.

Gessler P, Chadwick O, Chamran F, Althouse L, Holmes K. 2000. Modeling soil–landscape and ecosystem properties using terrain attributes. *Soil Science Society of America Journal* **64**: 2046–2056.

Heimsath AM, Chappell J, Dietrich WE, Nishiizumi K, Finkel RC. 2000. Soil production on a retreating escarpment in southeastern Australia. *Geology* **28**: 787–790.

Heimsath AM, Dietrich WE, Nishiizumi K, Finkel RC. 1997. The soil production function and landscape equilibrium. *Nature* **388** (6640): 358.

Heimsath AM, Dietrich WE, Nishiizumi K, Finkel RC. 1999. Cosmogenic nuclides, topography, and the spatial variation of soil depth. *Geomorphology* **27**(1–2): 151–172.

Heimsath AM, Dietrich WE, Nishiizumi K, Finkel RC. 2001. Stochastic processes of soil production and transport: erosion rates, topographic variation and cosmogenic nuclides in the Oregon Coast Range. *Earth Surface Processes and Landforms* **26**: 531–552.

Hungr O, Evans S, Bovis M, Hutchinson J. 2001. A review of the classification of landslides of the flow type. *Environmental & Engineering Geoscience* **7**: 221–238.

Jakob M, Hungr O, Jakob DM. 2005. *Debris-flow hazards and related phenomena (Vol. 739)*. Springer: Berlin.

Johnson K, Sitar N. 1990. Hydrologic conditions leading to debris-flow initiation. *Canadian Geotechnical Journal* **27**: 789–801.

Lane JW, White EA, Steele GV, Cannia JC, Williams J. 2008. Estimation of bedrock depth using the horizontal-to-vertical (H/V) ambient-noise seismic method. In *Near Surface – 14th EAGE European Meeting of Environmental and Engineering Geophysics*.

Lirer L, Pescatore T, Booth B, Walker GP. 1973. Two plinian pumice-fall deposits from Somma-Vesuvius, Italy. *Geological Society of America Bulletin* **84**: 759–772.

Lowe DJ, Tonkin PJ. 2010. Unravelling upbuilding pedogenesis in tephra and loess sequences in New Zealand using tephrochronology. In *Proceedings of the 19th World Congress of Soil Science "Soil Solutions for a Changing World"*, Gilkes RJ, Prakongkep N (eds). Symposium 1.3.2 Geochronological Techniques and Soil Formation: Brisbane; 34–37 http://www.iuss.org/19th%20WCSS/Author_Main.html.1–6 August 2010

McDaniel PA, Lowe DJ, Arnalds O, Ping CL. 2012. Andisols. In *Handbook of Soil Sciences. Second Edition. Volume 1: Properties and Processes*, Huang PM, Li Y, Sumner ME (eds), Vol. **33**. CRC Press: Boca Raton, FL; 29–33.48.

Mercogliano P, Segoni S, Rossi G, Sikorsky B, Tofani V, Schiano P, Catani F, Casagli N. 2013. A prototype forecasting chain for rainfall induced shallow landslides. *Natural Hazards and Earth System Science* **13**: 771–777.

Moore ID, Gessler P, Nielsen G, Peterson G. 1993. Soil attribute prediction using terrain analysis. *Soil Science Society of America Journal* **57**: 443–452.

Mudd SM, Furbish DJ. 2004. Influence of chemical denudation on hillslope morphology. *Journal of Geophysical Research: Earth Surface* **109**: F02001.

Nakamura Y. 1989. A method for dynamic characteristics estimation of subsurface using microtremor on the ground surface. *Railway Technical Research Institute, Quarterly Reports* **30**.

Napolitano E, De Vita P, Fusco F, Allocca V, Manna F. 2015. Long-term hydrological modelling of pyroclastic soil mantled slopes for assessing rainfall thresholds triggering debris flows: the case of the Sarno Mountains (Campania—southern Italy). In *Engineering Geology for Society and Territory–Volume 2*. Springer: Berlin; 1567–1570.

Napolitano E, Fusco F, Baum RL, Godt JW, De Vita P. 2016. Effect of antecedent-hydrological conditions on rainfall triggering of debris flows in ash-fall pyroclastic mantled slopes of Campania (southern Italy). *Landslides* **13**: 967–983.

Odeha I, McBratney A, Chittleborough D. 1994. Spatial prediction of soil properties from landform attributes derived from a digital elevation model. *Geoderma* **63**: 197–214.

Park S, McSweeney K, Lowery B. 2001. Identification of the spatial distribution of soils using a process-based terrain characterization. *Geoderma* **103**: 249–272.

Pazzi V, Morelli S, Fidolini F, Krymi E, Casagli N, Fanti R. 2016a. Testing cost-effective methodologies for flood and seismic vulnerability assessment in communities of developing countries (Dajç northern Albania). *Geomatics, Natural Hazards and Risk* **7**: 971–999. https://doi.org/10.1080/19475705.2015.1004374.

Pazzi V, Morelli S, Pratesi F, Sodi T, Valori L, Gambacciani L, Casagli N. 2016b. Assessing the safety of schools affected by geo-hydrologic hazards: the geohazard safety classification (GSC). *International Journal of Disaster Risk Reduction* **15**: 80–93. https://doi.org/10.1016/j.ijdrr.2015.11.006.

Pazzi V, Tanteri L, Bicocchi G, D'Ambrosio M, Caselli A, Fanti R. 2017a. H/V measurements as an effective tool for the reliable detection of landslide slip surfaces: case studies of Castagnola (La Spezia, Italy) and Roccalbegna (Grosseto, Italy). *Physics and Chemistry of the Earth* **98**: 136–153. https://doi.org/10.1016/j.pce.2016.10.014.

Pazzi V, Lotti A, Chiara P, Lombardi L, Nocentini M, Casagli N. 2017b. Monitoring of the vibration induced on the Arno masonry embankment wall by the conservation works after the May 25, 2016 riverbank landslide. *Geoenvironmental Disasters* **4**: 6. https://doi.org/10.1186/s40677-017-0072-2.

Pelletier JD, Rasmussen C. 2009. Geomorphically based predictive mapping of soil thickness in upland watersheds. *Water Resources Research* **45**: W09417. https://doi.org/10.1029/2008WR007319.

Perrotta A, Scarpati C. 2003. Volume partition between the plinian and co-ignimbrite air fall deposits of the Campanian Ignimbrite eruption. *Mineralogy and Petrology* **79**: 67–78.

Roering JJ, Kirchner JW, Dietrich WE. 1999. Evidence for nonlinear, diffusive sediment transport on hillslopes and implications for landscape morphology. *Water Resources Research* **35**: 853–870.

Rolandi G, Bertollini F, Cozzolino G, Esposito N, Sannino D. 2000. Sull'origine delle coltri piroclastiche presenti sul versante occidentale del Pizzo d'Alvano (Sarno-Campania). *Quaderni di Geologia Applicata* **7**: 37–48.

Rolandi G, Maraffi S, Petrosino P, Lirer L. 1993a. The Ottaviano eruption of Somma-Vesuvio (8000 y BP): a magmatic alternating fall and flow-forming eruption. *Journal of Volcanology and Geothermal Research* **58**: 43–65.

Rolandi G, Mastrolorenzo G, Barrella A, Borrelli A. 1993b. The Avellino plinian eruption of Somma-Vesuvius (3760 yBP): the progressive evolution from magmatic to hydromagmatic style. *Journal of Volcanology and Geothermal Research* **58**: 67–88.

Rolandi G, Petrosino P, Mc GJ. 1998. The interplinian activity at Somma–Vesuvius in the last 3500 years. *Journal of Volcanology and Geothermal Research* **82**: 19–52.

Rosi M, Principe C, Vecci R. 1993. The 1631 Vesuvius eruption. A reconstruction based on historical and stratigraphical data. *Journal of Volcanology and Geothermal Research* **58**: 151–182.

Rossi G, Catani F, Leoni L, Segoni S, Tofani V. 2013. HIRESSS: a physically based slope stability simulator for HPC applications. *Natural Hazards and Earth System Sciences* **13**: 151–166.

Saco PM, Willgoose GR, Hancock GR. 2006. *Spatial Organization of Soil Depths using a Landform Evolution Model| NOVA*. The University of Newcastle's Digital Repository: Newcastle.

Salciarini D, Godt JW, Savage WZ, Conversini P, Baum RL, Michael JA. 2006. Modeling regional initiation of rainfall-induced shallow landslides in the eastern Umbria Region of central Italy. *Landslides* **3**: 181–194.

Saulnier G-M, Beven K, Obled C. 1997. Including spatially variable effective soil depths in TOPMODEL. *Journal of Hydrology* **202**: 158–172.

Schumacher T, Lindstrom M, Schumacher J, Lemme G. 1999. Modeling spatial variation in productivity due to tillage and water erosion. *Soil and Tillage Research* **51**: 331–339.

Segoni S, Leoni L, Benedetti AI, Catani F, Righini G, Falorni G, Gabellani S, Rudari R, Silvestro F, Rebora N. 2009. Towards a definition of a real-time forecasting network for rainfall induced shallow landslides. *Natural Hazards and Earth System Sciences* **9**: 2119–2133. https://doi.org/10.5194/nhess-9-2119-2009.

Segoni S, Martelloni G, Catani F. 2013. Different methods to produce distributed soil thickness maps and their impact on the reliability of shallow landslide modeling at catchment scale. In *Landslide Science and Practice*. Springer: Berlin; 127–133.

Segoni S, Rossi G, Catani F. 2012. Improving basin scale shallow landslide modelling using reliable soil thickness maps. *Natural Hazards* **61**: 85–101.

Selby MJ. 1982. *Hillslope Materials and Processes*. Oxford University Press: Oxford.

SESAME. 2004. Guidelines for the implementation of the H/V spectral ratio technique on ambient vibrations. Measurements, processing and interpretation. SESAME European research project, WP12 – Deliverable D23.12, European Commission – Research General Directorate, Project No. EVG1-CT-2000-00026 SESAME.

Sparks RSJ, Bursik MI, Ablay GJ, Thomas RME, Carey SN. 1992. Sedimentation of tephra by volcanic plumes. Part 2: controls on thickness and grain-size variations of tephra fall deposits. *Bulletin of Volcanology* **54**: 685–695.

Tarquini S, Vinci S, Favalli M, Doumaz F, Fornaciai A, Nannipieri L. 2012. Release of a 10-m-resolution DEM for the Italian territory: Comparison with global-coverage DEMs and anaglyph-mode exploration via the web. *Computers & Geosciences* **38**: 168–170.

Taylor G, Eggleton RA. 2001. Regolith geology and geomorphology. Wiley, 384 pp.

Terribile F, Basile A, De Mascellis R, Di Gennaro A, Mele G, Vingiani S. 2000. I suoli delle aree di crisi di Quindici e Sarno: proprietà e comportamenti in relazione ai fenomeni franosi. *Quaderni di Geologia Applicata* **7**: 59–79.

Tesfa TK, Tarboton DG, Chandler DG, McNamara JP. 2009. Modeling soil depth from topographic and land cover attributes. *Water Resources Research* **45**: W10438.

Tsai C-C, Chen Z-S, Duh C-T, Horng F-W. 2001. Prediction of soil depth using a soil-landscape regression model: a case study on forest soils in southern Taiwan. *Proceedings of National Science Council Republic of China Part B Life Sciences* **25**: 34–39.

USDA. 1998. *Keys to Soil Taxonomy*. USDA: Washington, DC.

Van Asch TW, Buma J, Van Beek L. 1999. A view on some hydrological triggering systems in landslides. *Geomorphology* **30**: 25–32.

Vogel S, Märker M. 2013. Modeling the spatial distribution of AD 79 pumice fallout and pyroclastic density current and derived deposits of Somma-Vesuvius (Campania, Italy) integrating primary deposition and secondary redistribution. *Bulletin of Volcanology* **75**: 1–15.

Wu W, Sidle RC. 1995. A distributed slope stability model for steep forested basins. *Water Resources Research* **31**: 2097–2110.

